Chemical Engineering Science 298 (2024) 120370

Contents lists available at ScienceDirect

Chemical Engineering Science

journal homepage: www.elsevier.com/locate/ces

On the extraction of volatile fatty acids from food waste mixtures: Comparison between the use of liquid–liquid and magnetic nanoparticle technologies

Elisa Lacroce [a], Filippo Rossi [a,*], Andrea Gianico [b], Agata Gallipoli [b], Simone Gelosa [a], Valentina Busini [a], Camilla Maria Braguglia [b], Maurizio Masi [a,*]

[a] Department of Chemistry, Materials and Chemical Engineering "Giulio Natta", Politecnico di Milano, piazza Leonardo da Vinci 32, 20133 Milan, Italy
[b] CNR-IRSA, Water Research Institute, National Research Council, Via Salaria Km 29, 300, 00015 Monterotondo, Rome, Italy

ARTICLE INFO

Keywords:
Volatile fatty acids
Iron oxide
Liquid–liquid extraction
Nanoparticles
Sustainability

ABSTRACT

The extraction of volatile fatty acids (VFAs) from an aqueous solution derived by fermentation of food waste is a key challenge in the context of the circular economy, thanks to their high economic and environmental impact due to their wide-ranging use in various industrial fields. In this work, we compared two different extraction methods: one novel and one classical. Firstly, iron oxide nanoparticles of around 10 nm were prepared and used as they are or functionalised using (3-Aminopropyl)triethoxysilane) (APTES) molecules, adipic acid and oleic acid. This was compared with a traditional industrial method (liquid–liquid extraction) that can guarantee high extraction of VFAs with high reproducibility. Indeed the use of dichloromethane, hexane, methyl *tert*-butyl ether and oleic acid presented extraction values of up to 30 % while iron oxide NPs showed results with low reproducibility. The comparison demonstrated the use of oleic acid as a promising solvent for liquid–liquid extraction of VFAs.

1. Introduction

Volatile fatty acids (VFAs) are widely used in the chemical, pharmaceutical and food industries (Wu et al., 2023; Agnihotri et al., 2022; López-Garzón and Straathof, 2014; Yesil et al., 2021). They are short-chain carboxylic acids that contain from two to eight carbon atoms (Banel and Zygmunt, 2011; van den Bruinhorst et al., 2018). The continuous growth in market demand is due to their wide-ranging application for producing paint, plastics, synthetic fibres, emulsions, coating formulations, pesticides, flavours, supplements and antibiotics (Atasoy et al., 2018; Patel et al., 2021). About 90 % of VFA production is derived via petrochemical routes with negative effects on the environment (Atasoy et al., 2018; Fufachev et al., 2020). There are also bio-based production methods, but the high costs and the low efficiency resulting from inhibiting bacteria at low pH (Atasoy et al., 2018) limits their use. For these reasons interest in searching for alternative methods for VFA production is spreading. In particular, the recovery of chemical products from waste streams represents a promising strategy in the context of the circular economy (Hernandez et al., 2021; Lee et al., 2014; Awasthi et al., 2023; Witek-Krowiak et al., 2022). One method is represented by the so called *Carboxylate Platform*, based on converting organic feedstock from industrial and agricultural waste into short-chain carboxylates as chemical intermediates, by hydrolysis and fermentation under anaerobic conditions, and then into complex fuels (Yesil et al., 2021; Andersen et al., 2015; Yin et al., 2022; Sapmaz et al., 2022). The price of intermediate compounds is fifteen times higher per ton than fuels (Andersen et al., 2015) and, in turn, the increasing cost of petroleum-derived raw materials increases the commercial cost of VFAs (Zacharof and Lovitt, 2013). Various studies have been conducted on producing chemicals while reducing the environmental impact or avoiding petrochemical routes (Du et al., 2013; Garcia Alba et al., 2012; Luque et al., 2014; van Putten et al., 2013; Zakzeski et al., 2010). The idea of using the Carboxylate Platform in order to recover VFAs from food waste minimizes the negative effect of traditional VFA production on the environment and at the same time represents an economic advantage. As reported by FAO, 14 % of food, valued at an estimated USD 400 billion, is lost between being harvested and up to, but not including, retail. Seventeen percent more is wasted at the retail and

* Corresponding authors.
E-mail addresses: filippo.rossi@polimi.it (F. Rossi), maurizio.masi@polimi.it (M. Masi).

https://doi.org/10.1016/j.ces.2024.120370
Received 9 November 2023; Received in revised form 6 June 2024; Accepted 10 June 2024
Available online 12 June 2024

consumer levels (https://www.fao.org/policy-support/policy-themes/food-loss-food- waste/en). Every year about 1,3 billion tons of edible food waste are produced (https://www.fao.org/sustainable-food-value-chains/library/details/en/c/266053) and in Europe alone, about 129 million tons of food wastage are generated every year, of which 46 % is produced at the consumption stage followed by primary production (25 %), processing and manufacturing (24 %), and distribution and retailing (5 %) (Caldeira et al., 2019).

Nowadays, the organic fraction of solid waste can be treated in various ways. The increased cost resulting from European directives on landfilling has limited its use as a treatment method (Capson-Tojo et al., 2016), as it also leads to environmental issues such as leaching, greenhouse gasses and odour production. Aerobic digestion produces rich soil used as fertiliser in agriculture, but it produces a low value-added product (Capson-Tojo et al., 2016; Balasubramani et al., 2023). Its use is limited in most of countries and in Europe it represents only 8 % of all household food waste treatments (https://www.unep.org/resources/report/unep-food-waste-index-report-2021). However, the economic value of biogas and digestate is limited, spurring the development of alternative approaches to yield higher-value end-products represented by VFAs (Gianico et al., 2021; Xing et al., 2023). There are three principal methods used to recover VFAs from a solution: liquid–liquid extraction (LLE), adsorption and membrane separation (Emam et al., 2023; Emam et al., 2022; Abdelhameed et al., 2021; Abdelhameed et al., 2018; Reyhanitash et al., 2017). LLE is based on using two immiscible solvents in order to favour the passage of the product from one phase to the other based on their chemical potential (Ramos-Suarez et al., 2021; Alkaya et al., 2009). This is the most studied technology for recovering carboxylic acids (López-Garzón and Straathof, 2014) and the most practical method used when the carboxylic acid content in an aqueous solution is below 50 wt% (Reyhanitash et al., 2018). Membrane separation consists of using a semipermeable membrane able to separate the product (Reyes et al., 2020) selectively. The passage across the membrane can be driven by pressure, concentration gradients or an electrical field (Li et al., 2023; Mazumder et al., 2020). The adsorption method allows the interaction of the molecule from the liquid or gas phase with a surface (Atasoy et al., 2018; Reyhanitash et al., 2018). This work focuses on recovering VFAs from an aqueous solution, that mimics the composition of the fermentation broth derived from food waste. The complexity of using a mixture, instead of using single molecule solutions, focuses the attention on possible problems related to selectivity and mutual interactions in VFA extraction. In this framework we compared an innovative method based on the use of functionalised magnetite nanoparticles as adsorbent agents and a classical one based on the liquid–liquid extraction method (LLE). For the first method, magnetite nanoparticles (MNPs) were synthesised using the co-precipitation method from hydrated $FeCl_2$ and $FeCl_3$ (Eskandari and Hasanzadeh, 2021; Rozi et al., 2016). Three different molecules were then used for to coat of nanoparticles in order to exploit different interactions with the VFAs present in the liquid fermented solution.

(3-Aminopropyl)triethoxysilane (APTES) was chosen to allow an electrostatic interaction with the VFAs, while adipic acid (AA) and oleic acid (OA) were selected to have a hydrophobic interaction. The possibility of using magnetic NPs for this purpose can be very promising and was compared here with different solvents used for the liquid–liquid extraction technique.

2. Material and methods

2.1. Materials

Ethanol (≥99.8 %), formic acid (≥95 %), methanol (≥99.8 %), sodium acetate (≥99 %), sodium propionate (≥99 %), sodium butyrate (98 %), isobutyric acid (99 %), valeric acid (≥99 %), isovaleric acid (99 %), and sodium hexanoate (99–100 %) were obtained from SigmaAldrich®. APTES (99 %), Iron (II) chloride tetrahydrate ($FeCl_2{\cdot}4H_2O$, 98 %), Iron (III) chloride hexahydrate ($FeCl_3{\cdot}6H_2O$, 97 %), NaOH, anhydrous pellets (>98 %), oleic acid (OA) (>90 %) and adipic acid (AA) (>99 %), which are the materials adopted for the synthesis of MNPs and functionalised MNPs (F-MNPs), were bought from the same provider. 1 M HCl was purchased by Fisher chemical, Fisher Scientific®. A cationic exchange resin, specifically Amberlyst 15wet purchased from Rohm and Haas, was used.

2.2. Preparation of synthetic fermentation broth

Ethanol (C_2H_6O, MW = 46.07 g/mol, ≥99.8 %), sodium acetate ($C_2H_3NaO_2$, MW = 82.03 g/mol, ≥99 %), sodium propionate ($C_3H_5NaO_2$, MW = 96.06 g/mol, ≥99 %), sodium butyrate ($C_4H_7NaO_2$, MW = 110.09 g/mol, 98 %), isobutyric acid ($C_4H_8O_2$, MW = 88.11 g/mol, 99 %), valeric acid ($C_5H_{10}O_2$, MW = 102.13 g/mol, ≥99 %), isovaleric acid ($C_5H_{10}O_2$, MW = 102.13 g/mol, 99 %), and sodium hexanoate ($C_6H_{11}NaO_2$, MW = 138.14 g/mol, 99–100 %) were dissolved in 250 mL of distilled water obtaining a total amount of about 19000 ppm (mass based) reflecting a typical composition of an enhanced food waste fermentation broth targeted for caproate production (Table 1). The pH of the final solution was between 5 and 6.

2.3. Synthesis of Fe_3O_4 NPs

The co-precipitation method was used for the synthesis of MNPs. 1.057 g of $FeCl_2{\cdot}4H_2O$ and 2.523 g of $FeCl_3{\cdot}6H_2O$ were dissolved in 106.6 mL of deionized water and the solution was stirred at 100 °C and 400 rpm for 1 h, in a nitrogen atmosphere. Then, 33.3 mL of NaOH (9.98 M) were added to the reaction mixture, which was stirred for another 1 hour. At the end, the solution was cooled at room temperature and washed three times with distilled water. NPs were recovered at the bottom of the flask after every washing step using an external magnet (neodymium fishing magnet model NJD90 by Wukong®).

2.4. APTES@MNPs functionalisation

According to the procedure described by Feng et al. (Feng et al., 2008); 2.25 mL of APTES ($C_9H_{23}NO_3Si$, MW = 221.37 g/mol, 99 %) were added to 9 mL of 0.5 M HCl and the solution was heated at 45 °C for 20 min in order to remove the ethanol which is formed during the reaction. Finally, the solution was dried under a vacuum at 45 °C for 5 min.

A 1:4 M ratio between MNPs and hydrolysed APTES was selected for the functionalisation. 550 mg of MNPs were dissolved in 50 mL of deionized water and 2.12 g of hydrolysed APTES solution were added. The solution was stirred constantly for 5 h at 60 °C in a nitrogen atmosphere. After cooling at room temperature, the MNPs were washed once with deionized water and once with ethanol. Finally, they were dried in a vacuum.

2.5. OA@MNPs/AA@MNPs functionalisation

In this case, functionalisation of the nanoparticles was done in the

Table 1
Quantities of VFAs used in the synthetic solution representing the fermentation broth.

Compound	Quantity [g]	Concentration [ppm]	%
Ethanol	0.691	2765.6	14.4
Sodium acetate	1.334	5334.8	27.9
Sodium propionate	0.246	982.4	5.1
Isobutyric acid	0.0696	278.4	1.5
Sodium butyrate	0.628	2510	13.1
Isovaleric acid	0.0363	145.2	0.8
Valeric acid	0.345	1380	7.2
Sodium hexanoate	1.436	5743	30

same steps as those for MNPs synthesis. 0.478 g of adipic acid were added into 9.56 mL of water. For oleic acid, 4 mL of water and ethanol were added to 1.042 mL of oleic acid. After the addition of a 10 M NaOH solution in the MNPs synthesis reaction, the respective acid solution (OA/AA) was added and the reaction continued under the same conditions as MNPs synthesis. At the end the solution was cooled down, the reaction solvent was removed, and the particles were washed twice with 80 mL of deionized water.

2.6. Nps characterisation

An X-ray diffraction experiment was carried out by SAMM laboratory at Politecnico di Milano using an Empyrean diffractometer by Malvern Panalytical®, equipped with Cu radiation (K-Alpha1, wavelength = 1.54060 Å) and it was carried out at 25 °C.

Transmission electron microscopy micrographs were collected using a TEM-Zeiss LIBRA 200FE instrument, equipped with a 200 kV FEG, in column, second-generation omega filter for energy selective spectroscopy (EELS) and imaging (ESI), HAADF STEM facility, EDS probe for chemical analysis, and integrated tomographic HW and SW systems.

TEM specimens were prepared by dropping an aqueous solution of NPs onto a carbon-coated copper grid (300 mesh) and evaporating the solvent. The particle size distribution was estimated using the ITEM-TEM Imaging platform—Olympus Soft Imaging Solutions.

FT-IR analysis was performed using a Varian 640-IR spectrometer equipped with a single bounce ZnSe ATR accessory. The attenuated total reflection (ATR) technique was applied.

Thermogravimetric analysis (TGA) was done on lyophilised samples. The instrument was an SDT Q6000 PerkinElmer used with a temperature increase of 10 °C/min, starting from 30 °C and up to 900 °C.

Elemental analysis was performed on freeze dried samples using a COSTECH ECS 4010 instrument.

2.7. Adsorption and desorption tests using iron oxide nanoparticles

Dry nanoparticles were dispersed in 6 mL of the VFA solution at different concentrations (5 mg/mL, 10 mg/mL, 15 mg/mL, 23 mg/mL, 30 mg/mL) and stirred at 700 rpm for 5 min. Then, the NPs were collected from the bottom of the vial using a magnet and the supernatant was extracted. The extracted volume (5 mL) was treated as described in the following paragraph (2.7). The residual VFA solution remained after the adsorption was removed leaving a defined quantity before conducting the desorption tests. Methanol (6 mL) was selected as the desorption solvent for tests on OA@MNPs and AA@MNPs. A 1 M NaOH (6 mL) aqueous solution (pH 14) was tested for desorption on APTES@MNPs.

2.8. Liquid-liquid extraction (LLE)

Different solvents were used for the LLE: dichloromethane (DCM), methyl *tert*-butyl ether (MTBE), n-hexane and oleic acid. The extraction was performed by mixing 6 mL of VFA solution with 5 mL of solvent. After the separation of the two solvents the aqueous phase was recovered and analysed using a GC instrument as described before.

In case of oleic acid extraction, the VFA solution (10 mL) was acidified (pH = 3) and then mixed with 12 mL of solvent. The whole mixture was agitated for 3 min in a funnel extractor. The mixture was placed in a falcon and centrifuged for 4 min at 4500 rpm, in order to facilitate the separation of the two phases. After the separation, the aqueous solution was treated as described previously for the GC analysis. Scheme 1 shows the two different methods used to recover the VFAs from a fermentation broth mimic solution. On the left of the graph, Fe_3O_4 magnetic nanoparticles were synthetised using the co-precipitation method and functionalised using APTES, adipic acid or oleic acid. Functionalised NPs were added to a VFA water solution to facilitate adsorption of the VFA molecules on the surface of NPs, which were collected using a magnet at the end of the process. On the right of scheme 1, the liquid–liquid extraction method was investigated using different organic solvents to extract the VFAs from the water phase.

2.9. Sample preparation for GC analysis

Some of compounds used were in their acidic form, whereas others were used as sodium salt derivatives. The accumulation of salt derivatives in the injector of the GC instrument can affect analysis and correct quantification of VFAs, so a cationic exchange resin (Amberlyst

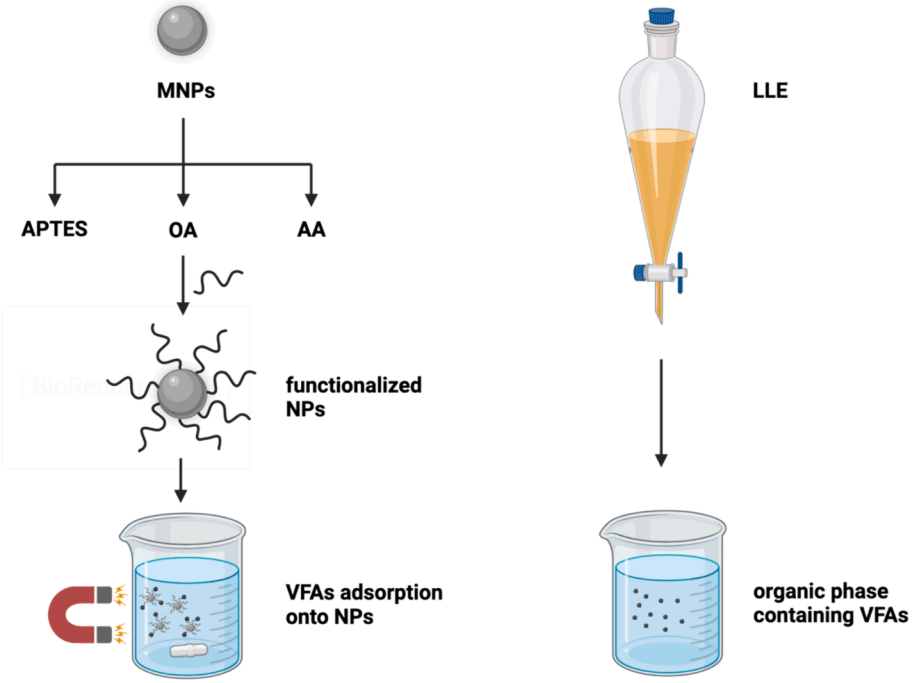

Scheme 1. Graphic representation of the two approaches used to remove VFAs from the fermentation broth mimic solution.

15wet) was used before GC analysis in order to remove the sodium ions in the solution. 6.845 g of resin were conditioned using 1 M HCl, charging the active sites with H + ions in order to replace the Na + in the VFA solution, and finally the resin was washed with water. The efficiency of this treatment was assessed by ICP, confirming a pre and post treatment sodium content of 2986 mg/L and 3.66 mg/mL respectively. Before every GC analysis, 5 mL of VFA sample solution were passed through the resin and diluted in deionized water up to 25 mL (1:5 dilution). 2.5 mL of diluted solution was then diluted using methanol (1:4 dilution) and 1 mL was taken for the GC analysis with the addition of 10 μL of formic acid. Analyses were performed on a Claurs 600 Gas Chromatograph equipped with a flame ionisation detector, helium was used as the carrier gas and the capillary column was a TRACE-FFAP 260N142P purchased from Thermo Fisher Scientific. The injector and carrier gas temperatures were set at 250 °C and 165 °C, respectively. The temperature of the oven was initially set at 40 °C for the first two minutes, then increased 10 °C/min for 18 min up to 220 °C. The temperature of 220 °C was maintained for the last 4 min.

2.10. Statistical analysis

All the experiments were carried out in triplicate and the data presented shows the mean values of independent experiments. Standard deviations are indicated wherever necessary.

3. Results and discussion

3.1. Morphological and physical characterisation of MNPs

Iron oxide NPs were prepared and functionalised using APTES, OA and AA as reported in the Materials and Methods section. TEM analysis of MNPs (Fig. 1a) and APTES@MNPs (Fig. 1b) showed a spherical shape and uniform size distribution with an average diameter of 13.4 nm and 12.2 nm respectively. AA@MNPs and OA@MNPs (Fig. 1c and 1d) showed a cubic shape derived from the different type of synthesis as reported in literature (Masur et al., 2016; Chen et al., 2012), which includes the functionalisation reaction during nanoparticle formation for both AA@MNPs and OA@MNPs. The dimensions of the NPs were also measured using DLS (Dynamic Light Scattering) analysis after being dissolved in distilled water, but their flocculated state does not allow reliable results to be obtaind due to the agglomeration that does not make it possible to obtain the values of primary particles (Table 2). In Table 2 the comparison between the diameter values obtained using DLS and TEM analyses can be seen. The average diameter sizes were 10.9 nm and 9.2 nm for AA@MNPs and OA@MNPs respectively. MNPs were also analysed from the point of view of crystallinity using XRD (Figure S1). Peaks at 2θ values of 18.27°, 30.13°, 35.44°, 43.21°, 53.44°, 56.90° and 62.65° were related to the iron oxide (Fe_3O_4) pattern. The crystal phase of Fe_3O_4 NPs matched that of magnetite demonstrating good crystallinity. FT-IR analysis was performed in order to verify surface functionalisation of MNPs. In Fig. 2 peaks between 550–600 cm^{-1} represent the Fe-O stretching vibration from iron oxide (**1**), the peak near 1600 cm^{-1} is related to the O-H deformed vibration (**2**) and that at 3400 cm^{-1} to the O-H stretching vibration (**3**) of MNPs.

The spectrum of APTES@MNPs shows a similar peak for Fe-O stretching vibration, whereas the more marked band between 3200–3400 cm^{-1} and 1600 cm^{-1} are related to the N-H stretching vibration and NH_2 bending mode of amine groups respectively. The intensity of nearly 1000 cm^{-1} relates to the Si–O stretching vibration.

Table 2
DLS and TEM analyses for MNPs and F-MNPs in terms of mean diameter.

	DLS	TEM
MNPs	140 ± 45	13.4 ± 2.5
APTES@MNPs	210 ± 65	12.2 ± 3
AA@MNPs	85 ± 20	10.9 ± 2.5
OA@MNPs	45 ± 15	9.2 ± 2.5

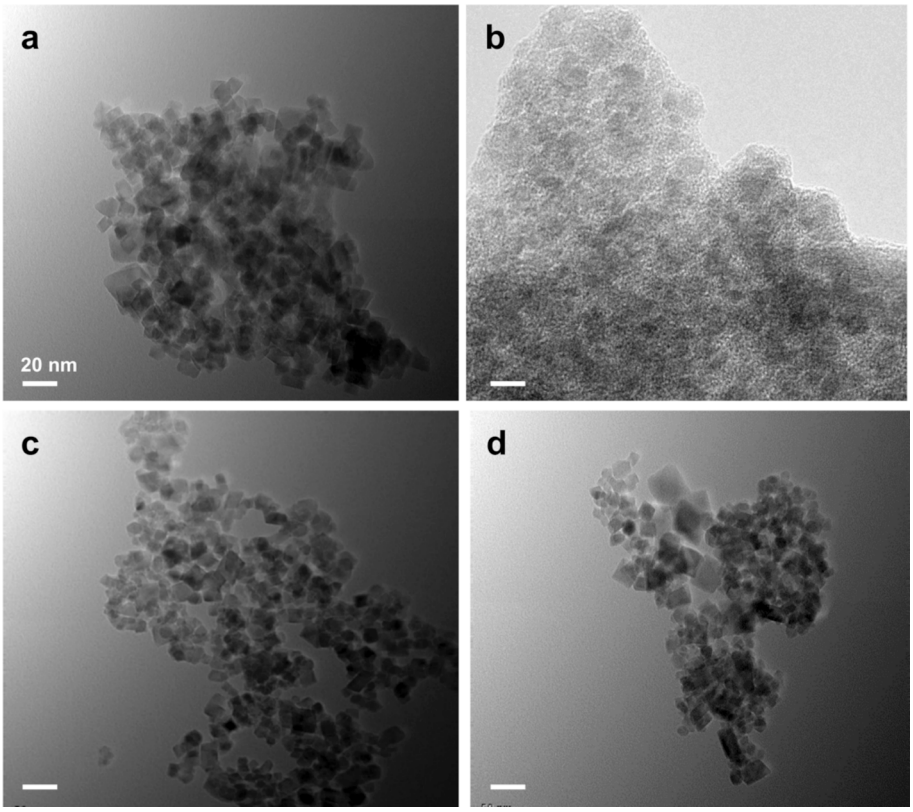

Fig. 1. TEM images of MNPs (a), APTES@MNPs (b), AA@MNPs (c) and OA@MNPs (d). (a, b, c, d) scale bars = 20 nm.

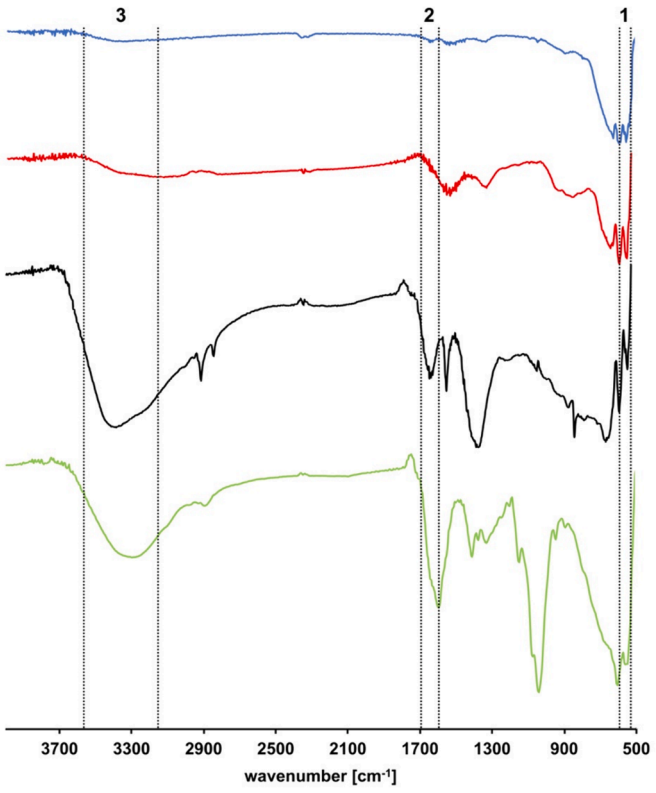

Fig. 2. FT-IR analysis of MNPs (blue), APTES@MNPs (green), AA@MNPs (red) and OA@MNPs (black). (For interpretation of the references to colour in this figure legend, the reader is referred to the web version of this article.)

Lastly the peak at 2800–3000 cm^{-1} and the value of nearly 1400 cm^{-1} show the $–CH_2$ and C–N stretching vibrations, respectively (Can et al., 2009; Shen et al., 2004). The spectrum of OA@MNPs and AA@MNPs presents two peaks at 1457 and 1557 cm^{-1} related to the symmetric and asymmetric stretching vibration of COO^- groups (Jadhav et al., 2013; Baharuddin et al., 2018). The first one of the two was also influenced by the overlapping with CH_2 scissoring of the carbon chain. In the OA@MNPs the peak at around 1700 cm^{-1} is correlated to the C=O bond stretching vibration of unbound oleic acid. The two distinct peaks between 2852 and 2922 cm^{-1} are due to symmetric and asymmetric stretching of C–H bond respectively, typical of the unsaturation inside the carbon chain (Wen et al., 2012).

In addition, elemental analysis was performed to verify the presence of functionalisation. The results are shown in Table 3. The presence of nitrogen in the APTES@MNPs sample demonstrated the effect of nanoparticle functionalisation. In addition, the increment in carbon and hydrogen compared with that of MNPs reflected the presence of the APTES on the surface of the NPs. The percentage of functionalisation of APTES@MNPs was estimated by establishing a ratio between the number of amine groups and that of the –OH groups present on MNPs. As reported by Olariu et al. (Olariu et al., 2011), the number of ligand on the surface of each nanoparticle is obtained using the formula $N = \omega N_A \rho V/MW$, where N is the number of ligands, ω is the mass loss in percent, N_A is Avogadro's number, ρ is the density of the nanoparticle, V is the volume of particle, and MW is the molecular weight of the ligand. By establishing the ratio between the two formulas, the resulting percentage of functionalisation F is shown by eq.1:

$$F = \frac{\omega_N * MW_H}{\omega_H * MW_N} * 100 = \frac{1*1\left(\frac{g}{mol}\right)}{0.93*14\left(\frac{g}{mol}\right)} * 100 = 7.7\% \quad (1)$$

This equation is based on considering only one linkage between the APTES and –OH group. In reality, it could be possible that the same molecule of APTES is linked with more than one –OH group and, at the same time, that molecules of APTES are linked together forming a silane polymer. In conclusion, the equation can only be used to make a qualitative evaluation. The content of carbon atoms derived from the CHNS analysis of OA@MNPs and AA@MNPs verified the presence of functional groups and showed a higher carbon content for OA@MNPs due to its higher molecular weight. For these last cases the percentage of functionalisation was not considered due to the unknown starting number of –OH groups on the surface of the NPs.

Z-potential analysis revealed a shift in the isoelectric point of functionalised NPs compared to the unfunctionalized ones (Fig. 3). In particular, functionalisation with APTES molecules modified the charge around the MNPs because of the presence of amine groups. The Z-potential of MNPs and F-MNPs dissolved in aqueous solutions at pH values of 2, 4, 6, 8 and 10 were measured. As shown in Fig. 3, the isoelectric point shifted from pH of around 5 to pH 9 making the nanoparticles positively charged up to pH 8 and negatively charged above pH 10. This, together with the FT-IR and CHNS results, confirmed that the surface had been effectively functionalised resulting in the attachment of APTES bearing amine functional groups (Nor et al., 2022; Karade et al., 2021). The isoelectric point of OA@MNPs and AA@MNPs was found to be near pH 6.5, more similar to that of MNPs with a positive charge below and a negative charge above this value.

TGA analysis (Fig. 4) of OA@MNPs and AA@MNPs showed initial weight percentage losses at around 100 °C related to the water loss adsorbed onto the surface of NPs (Jadhav et al., 2013; Wen et al., 2012). The second weight losses of 11 % and 3.48 % relate to the adsorbed oleic and adipic acid on the surface respectively, whereas the third weight losses related to molecules chemically bound to the surface of 9.12 % and 11.96 % for oleic and adipic acid respectively. A similar trend is presented in the TGA analysis of APTES@MNPs. In this case the total weight loss is lower (9.27 %) than that for OA@MNPs and AA@MNPs. This could be due to the low molecular weight of the APTES molecule or to the lower percentage functionalisation.

Table 3
CHN elemental analysis for MNPs and F-MNPs.

	N [%]	C [%]	H [%]
MNPs	<dl	1.2	0.9
APTES@MNPs	1.0	3.5	1.1
OA@MNPs	<dl	15.4	7.1
AA@MNPs	<dl	2.6	0.8

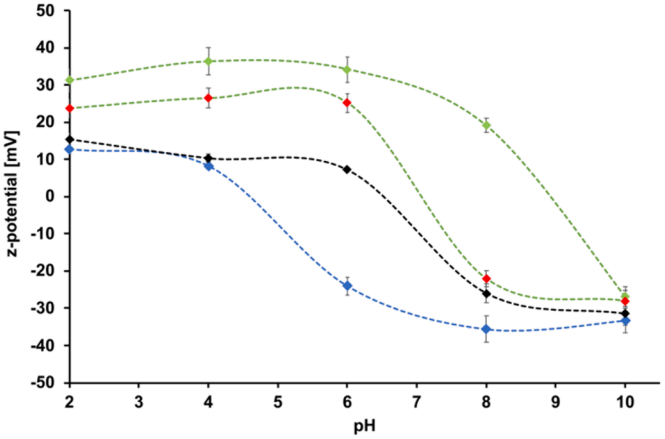

Fig. 3. Z-potential of MNPs (blue), APTES@MNPs (green), AA@MNPs (red) and OA@MNPs (black). (For interpretation of the references to colour in this figure legend, the reader is referred to the web version of this article.)

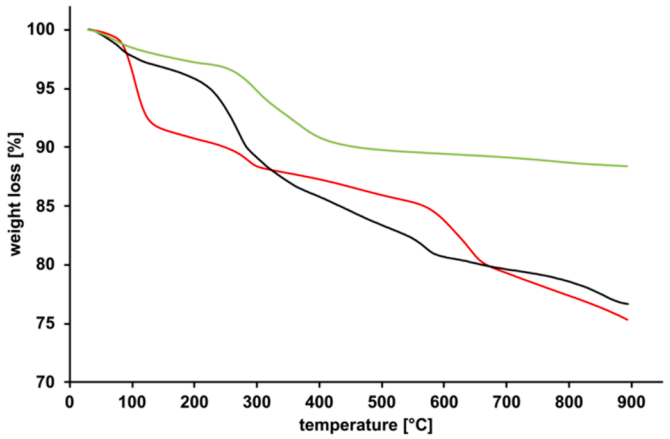

Fig. 4. TGA analysis of APTES@MNPs (green), AA@MNPs (red) and OA@MNPs (black). (For interpretation of the references to colour in this figure legend, the reader is referred to the web version of this article.)

3.2. Adsorption/desorption tests

Tests on adsorption properties were done by dissolving NPs at different concentrations (5 mg/mL, 10 mg/mL, 15 mg/mL, 23 mg/mL, 30 mg/mL) in the VFA solution. The time involved comes from optimisation tests with the final aim of increasing contact between VFAs and NPs on one side but also makes this choice competitive in terms of the time required on the other. The quantification of each VFA in the solution, after and before adsorption, was measured by GC analysis after proper calibration of the instrument with each VFA (Gazzola et al., 2022). The percentage of adsorption for each VFA was calculated using eq.

$$\%A_i = \frac{c_i \bullet A_{t0_i} - c_i \bullet A_{ads_i}}{c_i \bullet A_{t0_i}} \bullet 100 \quad (2)$$

Where i is the i-th acid and t0 refer to the VFA solution before adsorption. ads_i refers to the i-th acid after adsorption, c_i refers to the coefficients of the calibration curve for the i-th acid for the GC analysis, and A is the area resulting from integration of the peaks in the GC chromatograms. Fig. 5 revealed low adsorption percentages when using MNPs, with values of between 5 and 10 % at the lower MNPs concentrations. At higher concentrations of NPs no relevant adsorption values were registered. Higher percentage of adsorption was obtained for APTES@MNPs and AA@MNPs reaching values between 25 and 30 % at 5 and 10 mg/mL concentrations, whereas about 20 % of adsorption was calculated for OA@MNPs. No adsorption dependence on the concentration of nanoparticles was revealed and no selective VFA adsorption was verified. Adsorption tests at the optimal adsorption concentrations for APTES@MNPs (10 mg/mL), OA@MNPs (5 mg/mL) and AA@MNPs (5 mg/mL) were replicated in order to evaluate the effective adsorption capacity of nanoparticles and the results obtained showed high standard deviation underlining the low reliability of the measurements. Desorption tests were conducted to confirm the results obtained. The solvent used for the desorption tests was changed depending on the type of functionalisation. Methanol was used in the case of AA@MNPs and OA@MNPs, whereas an alkaline solution (NaOH 1 M) was used for APTES@MNPs in order to allow electrostatic repulsion between protonated VFAs and negatively charged nanoparticles. The desorption % was computed using the following formula:

$$\%D_i = \frac{F_{dil,des} A_{des_i} V_{des} c_i - F_{dil,residue} A_{ads_i} V_{residue} c_i}{F_{dil,t0} A_{t0_i} V_{t0} c_i - F_{dil,ads} A_{ads_i} V_{ads} c_i} \bullet 100 \quad (2)$$

Where *I* refers to the i-th acid, ads_i to the i-th acid of the VFA solution after adsorption, des_i to the i-th acid of the VFA solution after desorption,

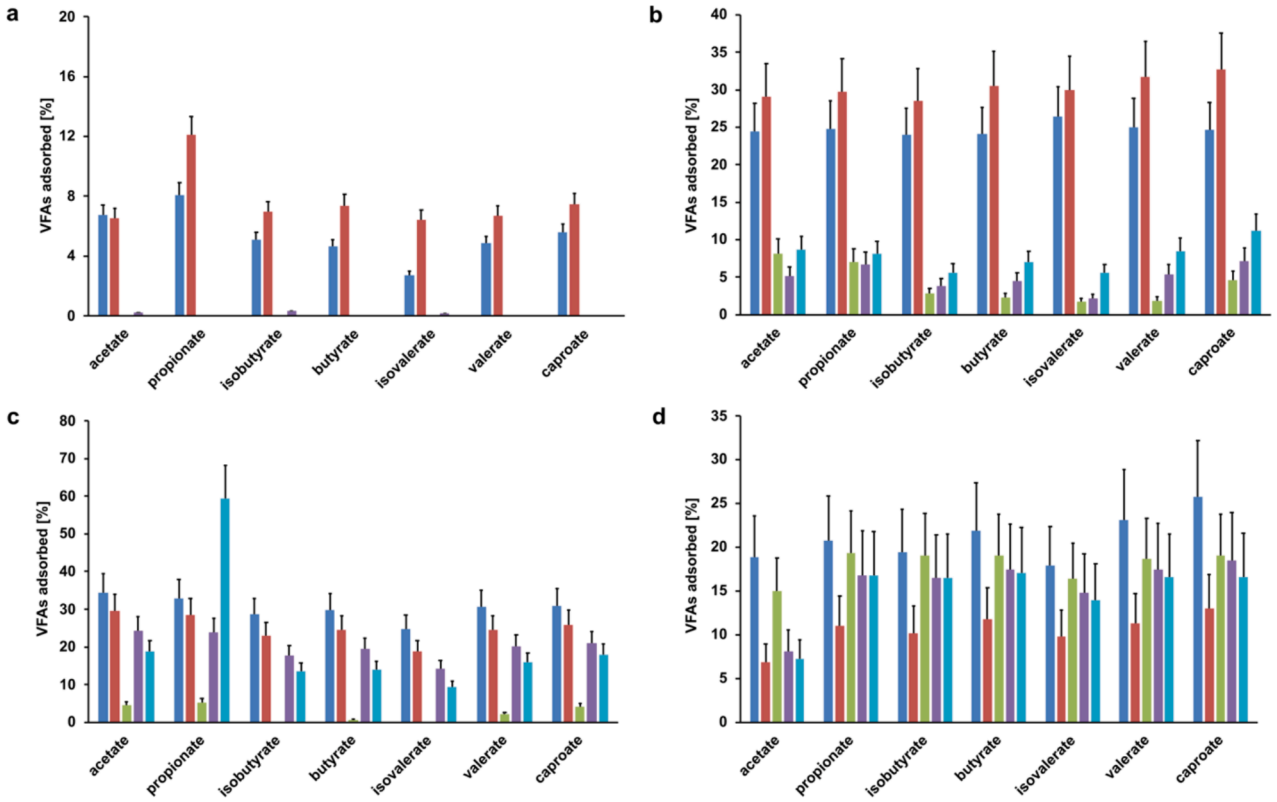

Fig. 5. Adsorption percentages of each VFA at 5 mg/mL (blue), 10 mg/mL (red), 15 mg/mL (green), 25 mg/mL (purple), 30 mg/mL (light blue) concentration of MNPs (a), APTES@MNPs (b), AA@MNPs (c) and OA@MNPs (d) (n = 3, mean value ± standard deviation). (For interpretation of the references to colour in this figure legend, the reader is referred to the web version of this article.)

F_{dil} to the dilution factor, c_i to the coefficients of the calibration curve for the i-th acid, A to the area resulting from integration of the peaks in the GC chromatograms and V to the volume.

The subscripts t_0, *ads*, *des* and *residues* refer to the starting VFA solution, after adsorption, after desorption, and the residue of the adsorption test, respectively. The results of the desorption tests were all between 0 and 1.7 %, confirming the low efficiency of desorption. In addition, for those tests with higher adsorption efficiency (20–30 %), the subsequent desorption tests indicated VFA concentrations that reflected those for $V_{residue}$. In this case the desorption capacity from NPs was found to be very low and ineffective. The percentages of extraction varied between 4 % and 16 % for all short-chain VFAs, irrespective of the solvent used. On the contrary, the extraction of caproate was significantly higher, reaching a maximum of 34 % with MTBE extraction. The lowest extraction percentage for all VFAs was obtained in the case of hexane solvent. The same result is reported in the work by Begum et al. (Begum et al., 2020), in which adsorption tests for formic acid, acetic acid, propionic acid and butyric acid performed using hexane had the lowest extraction efficiency compared to other six different solvents. As reported in literature (Begum et al., 2020), the use of DCM had higher extraction efficiency than that with hexane, but no significant extractions (around 15 %) were obtained.

3.3. Liquid-liquid extraction (LLE)

Finally, a comparison with a typical chemical engineering operation was done using liquid–liquid extraction (LLE). Indeed the use of nanoparticles, even if promising in several industrial fields, is far from the real application due to problems related to reliability in manufacture, costs and toxicity (Pinelli et al., 2023; Xuan et al., 2023). On the other hand, LLE, also used in several industrial recovery strategies (Reyhanitash et al., 2018; Qiao et al., 2023), is a mature technology nowadays, and is commonly used in many different industrial sectors. The results of the different VFA extraction tests using DCM, MTBE and hexane are shown in Fig. 6. They were selected as extractant solvents because there are organic and immiscible with the aqueous phase in which the VFAs are dissolved. DCM is one of the most widely used volatile organic compounds (VOCs) for industrial and analytical applications (Fu et al., 2006; Shehata et al., 2016) together with n-hexane, which is mostly used for the high extraction property on lipids, fatty acids and hydrophobic compounds (Farajzadeh and Abbaspour, 2018; Farajzadeh and Abbaspour, 2017). The use of MTBE is less diffused compared to DCM and hexane, but is still used as an extraction solvent when preparing samples for analytical tests (Wu et al., 2010; Zhu et al., 2012).

It is clear that extraction of compounds is possible using all the solvents considered with the highest performance being recorded with DCM for all the VFAs present within the food waste mixture. Hexane and MTBE, on the contrary, being less polar showed less ability to extract VFA compounds. Of these, MTBE, thanks to its higher polarity, can guarantee values for valerate and caproate comparable to those obtained using DCM. In general, the extraction values increase with the carbon chain length of the VFA molecule, resulting in higher hydrophobic interactions between VFAs and the solvent. In order to find a greener solution, oleic acid was tested as an alternative due to its compatibility and safe use (Nistor et al., 2016; de Oliveira Camargo and J.L. Castagnari Willimann Pimenta, M. de Oliveira Camargo, P.A. Arroyo, , 2020). The results related to average and standard deviation values for VFA extraction using oleic acid are shown in Fig. 7. The extraction values for VFAs using oleic acid were much higher than those obtained using functionalised magnetic nanoparticles, although only one passage of LLE was performed for each extraction. The choice of using a single passage was based on the need to compare the two techniques considered in this work. In addition it is clear here that the low values of standard deviation obtained indicate high reproducibility of the technique considered.

All the compounds considered presented extraction values above 30 %, with the only exception being acetate. In this case too, the low values of standard deviation obtained indicated high reproducibility of the technique. The extracted values increased with the increase of carbon atoms present in the VFA molecule with a maximum value of 97 % that was reached for the caproate molecule due to the higher hydrophobic interactions with oleic acid. This result is also in agreement with the recent work of Yuan and coworkers, where they reported higher extraction values of caprylic acid (C8) compared to caproic acid (C6) performed under the same extraction conditions using eight different solvents (Yuan et al., 2023). This is due to the electron-releasing effect of the alkyl group, which increases with the increase of chain length, leading to higher electron density at the carbonyl carbon. This fact depolarises the bond between the oxygen and the hydrogel and obstructs the release of protons from the hydroxyl group. This effect is a higher

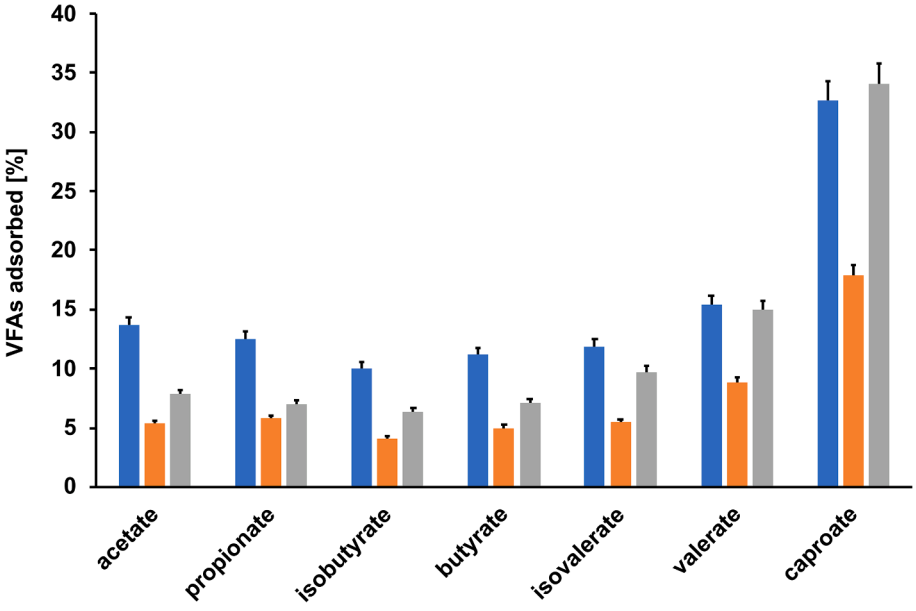

Fig. 6. Extraction average for each VFA using DCM (blue), hexane (orange), MTBE (grey) (n = 3, mean value ± standard deviation). (For interpretation of the references to colour in this figure legend, the reader is referred to the web version of this article.)

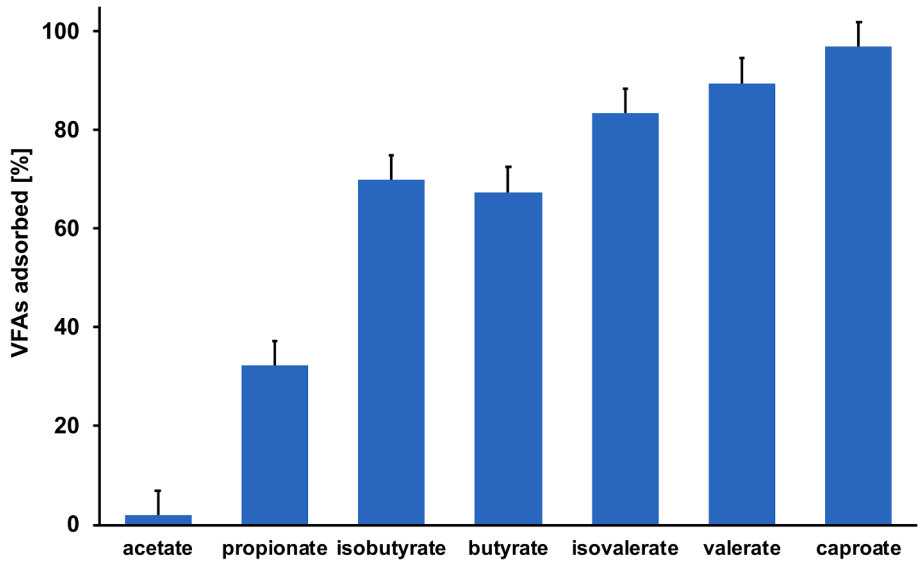

Fig. 7. LLE percentages and st.dev of each VFA using oleic acid. (n = 3, mean value ± standard deviation).

presence of undissociated compounds, with a consequent higher percentage of extraction for the compounds characterised by higher chain length (Yuan et al., 2023). High extraction values were also reached for isovalerate and valerate (above 80 %).

4. Conclusions

The experiments discussed above compared two different options that can be used in the extraction of VFA molecules from food waste mixtures obtained after fermentation. Firstly magnetic iron oxide nanoparticles were synthesised using the co-precipitation method from hydrated ferrous and ferric chloride and were then used neat or functionalised. The adsorption tests done on VFA liquid mixtures underlined higher performance of functionalised NPs than the neat ones. However, although promising, the low reproducibility of the results obtained, together with the problems related to VFA desorption, limit their use. The second technique considered is represented by LLE, a commonly known industrial traditional method, that, in the case studied in this work, is able to guarantee high extraction of VFAs with high values of reproducibility. Of these the highest extraction values were registered using oleic acid (green solvent) as the extraction solvent with the maximum value recorded for caproate (97 %) and an average extraction value of around 65 % with only a single cycle. These results demonstrated that the use of oleic acid is extremely promising while the use of magnetic NPs still presents many challenges that must be solved before considering it as a mature alternative for industrial applications.

CRediT authorship contribution statement

Elisa Lacroce: Methodology, Validation, Writing – original draft. **Filippo Rossi:** Conceptualization, Supervision, Writing – review & editing. **Andrea Gianico:** Methodology. **Agata Gallipoli:** Methodology. **Simone Gelosa:** Methodology. **Valentina Busini:** Methodology, Writing – review & editing. **Camilla Maria Braguglia:** Methodology, Validation. **Maurizio Masi:** Conceptualization, Supervision, Writing – review & editing.

Declaration of competing interest

The authors declare that they have no known competing financial interests or personal relationships that could have appeared to influence the work reported in this paper.

Data availability

Data will be made available on request.

Acknowledgments

This paper is dedicated to Massimo Morbidelli, who was a mentor for the entire PoliMI team, on the occasion of his 70th birthday. All the authors are grateful for the financial support obtained from Fondazione Cariplo, via the REVENUE project “3-routes platform for REcovery of high Value products, Energy and bio-fertilizer from Urban biowastE”, Contract #2019-2407.

Appendix A. Supplementary data

Supplementary data to this article can be found online at https://doi.org/10.1016/j.ces.2024.120370.

References

Abdelhameed, R.M., El-deib, H.R., El-Dars, F.M.S., Ahmed, H.B., Emam, H.E., 2018. Applicable strategy for removing liquid fuel nitrogenated contaminants using MIL-53-NH2@natural fabric composites. Ind. Eng. Chem. Res. 57, 15054–15065.

Abdelhameed, R.M., Alzahrani, E., Shaltout, A.A., Emam, H.E., 2021. Temperature-controlled-release of essential oil via reusable mesoporous composite of microcrystalline cellulose and zeolitic imidazole frameworks. J. Ind. Eng. Chem. 94, 134–144.

Agnihotri, S., Yin, D.M., Mahboubi, A., Sapmaz, T., Varjani, S., Qiao, W., Koseoglu-Imer, D.Y., Taherzadeh, M.J., 2022. A glimpse of the world of volatile fatty acids production and application: a review bioengineered. Bioengineered 13, 1249–1275.

Alkaya, E., Kaptan, S., Ozkan, L., Uludag-Demirer, S., Demirer, G.N., 2009. Recovery of acids from anaerobic acidification broth by liquid–liquid extraction. Chemosphere 77, 1137–1142.

Andersen, S.J., Candry, P., Basadre, T., Khor, W.C., Roume, H., Harnandez-Sanabria, E., Coma, M., Rabaey, K., 2015. Electrolytic extraction drives volatile fatty acid chain elongation through lactic acid and replaces chemical pH control in thin stillage fermentation. Biotechnol. Biofuels Bioprod. 8, 221.

Atasoy, M., Owusu-Agyeman, I., Plaza, E., Cetecioglu, Z., 2018. Bio-based volatile fatty acid production and recovery from waste streams: Current status and future challenges. Bioresour. Technol. 268, 773–786.

Awasthi, M.K., Ganeshan, P., Gohil, N., Kumar, V., Singh, V., Rajendran, K., Harirchi, S., Solanki, M.K., Sindhu, R., Binod, P., Zhang, Z., Taherzadeh, M.J., 2023. Advanced approaches for resource recovery from wastewater and activated sludge: A review. Bioresour. Technol. 384, 129250.

Baharuddin, A.A., Ang, B.C., Hussein, N.A.A., Andriyana, A., Wong, Y.H., 2018. Mechanisms of highly stabilized ex-situ oleic acid-modified iron oxide nanoparticles functionalized with 4-pentynoic acid. Mater. Chem. Phys. 203, 212–222.

Balasubramani, R., Awasthi, M.K., Varjani, S., Karmegam, N., 2023. Aerobic and Anaerobic digestion of agro-industrial and livestock wastes: a green and sustainable way toward the future. Agronomy 13, 2607.

Banel, A., Zygmunt, B., 2011. Application of gas chromatography-mass spectrometry preceded by solvent extraction to determine volatile fatty acids in wastewater of municipal, animal farm and landfill origin. Water Sci. Technol. 63, 590–597.
Begum, S., Arelli, V., Anupoju, G.R., Sridhar, S., Bhargava, S.K., Eshtiaghi, N., 2020. Optimization of feed and extractant concentration for the liquid-liquid extraction of volatile fatty acids from synthetic solution and landfill leachate. J. Ind. Eng. Chem. 90, 190–202.
Caldeira, C., De Laurentiis, V., Corrado, S., van Holsteijn, F., Sala, S., 2019. Quantification of food waste per product group along the food supply chain in the European Union: a mass flow analysis. Resour. Conserv. Recycl. 149, 479–488.
Can, K., Ozmen, M., Ersoz, M., 2009. Immobilization of albumin on aminosilane modified superparamagnetic magnetite nanoparticles and its characterization. Coll. Surf. B BIointerfaces 71, 154–159.
Capson-Tojo, G., Rouez, M., Crest, M., Steyer, J.P., Delgenes, J.P., Escudiè, R., 2016. Food waste valorization via anaerobic processes: a review. Rev. Environ. Sci. Biotechnol. 15, 499–507.
Chen, Y.H., Chi, M.C., Wang, T.F., Chen, J.C., Lin, L.L., 2012. Preparation of magnetic nanoparticles and their use for immobilization of C-terminally lysine-tagged Bacillus sp. TS-23 α-amylase. Appl. Biochem. Biotechnol. 166, 1711–1722.
de Oliveira Camargo, M., Castagnari Willimann Pimenta, J.L., de Oliveira Camargo, M., Arroyo, P.A., 2020. Green diesel production by solvent-free deoxygenation of oleic acid over nickel phosphide bifunctional catalysts: Effect of the support. Fuel 281, 118719.
Du, Y., Schuur, B., Samorì, C., Tagliavini, E., Brilman, D.W.F., 2013. Secondary amines as switchable solvents for lipid extraction from non-broken microalgae Bioresour. Technol. 149, 253–260.
Emam, H.E., El-Shahat, M., Taha, M., Abdelhameed, R.M., 2022. Microwave assisted post-synthetic modification of IRMOF-3 and MIL-68-NH2 onto cotton for Fuel purification with computational explanation. Surf. Interf. 30, 101940.
Emam, H.E., Ahmed, H.B., El-Shahat, M., Abdel-Gawad, H., Abdelhameed, R.M., 2023. Selective separation of chlorophyll-a using recyclable hybrids based on Zn-MOF@ cellulosic fibers. Sci. Rep. 13, 15208.
Eskandari, M.J., Hasanzadeh, I., 2021. Size-controlled synthesis and characterization of Fe3O4 nanoparticles by chemical coprecipitation method. Mater. Sci. Eng. B 266, 115050.
Farajzadeh, M.A., Abbaspour, M., 2017. Development of a new sample preparation method based on liquid–liquid–liquid extraction combined with dispersive liquid–liquid microextraction and its application on unfiltered samples containing high content of solids. Talanta 174, 111–121.
Farajzadeh, M.A., Abbaspour, M., 2018. Development of new extraction method based on liquid–liquid–liquid extraction followed by dispersive liquid–liquid microextraction for extraction of three tricyclic antidepressants in plasma samples. Biomed. Chromatogr. 32, e4251.
Feng, B., Hong, R.Y., Wang, L.S., Guo, L., Li, H.Z., Ding, J., Zheng, Y., Wei, D.G., 2008. Synthesis of Fe3O4/APTES/PEG diacid functionalized magnetic nanoparticles for MR imaging. Coll. Surf. A Physicochem Eng. Asp. 328, 52–59.
Fu, X., Dai, S., Zhang, Y., 2006. Comparison of extraction capacities between ionic liquids and dichloromethane. Chinese J. Anal. Chem. 34, 589–602.
Fufachev, E.V., Weckhuysen, B.M., Bruijnincx, P.C.A., 2020. Toward catalytic ketonization of volatile fatty acids extracted from fermented wastewater by adsorption. ACS Sustain. Chem. Eng. 8, 11292–11298.
Garcia Alba, L., Torri, C., Samorì, C., van der Spek, J., Fabbri, D., Kersten, S.R.A., Brilman, D.W.F., 2012. Hydrothermal Treatment (HTT) of microalgae: evaluation of the process as conversion method in an algae biorefinery concept. Energy Fuels 26, 642–657.
Gazzola, G., Braguglia, C.M., Crognale, S., Gallipoli, A., Mininni, G., Piemonte, V., Rossetti, S., Tonanzi, B., Gianico, A., 2022. Biorefining food waste through the anaerobic conversion of endogenous lactate into caproate: A fragile balance between microbial substrate utilization and product inhibition. Waste Manag. 150, 328–338.
Gianico, A., Gallipoli, A., Gazzola, G., Pastore, C., Tonanzi, B., Braguglia, C.M., 2021. A novel cascade biorefinery approach to transform food waste into valuable chemicals and biogas through thermal pretreatment integration. Bioresour. Technol. 338, 125517.
Hernandez, P.A., Zhou, M., Vassilev, I., Freguia, S., Zhang, Y., Keller, J., Ledezma, P., Virdis, B., 2021. Selective extraction of medium-chain carboxylic acids by electrodialysis and phase separation. ACS Omega 6, 7841–7850.
Jadhav, N.V., Prasad, A.I., Kumar, A., Mishra, R., Chara, S., Babu, K.R., Prajapat, C.L., Misra, N.L., Ningthoujam, R.S., Pandey, B.N., Vatsa, R.K., 2013. Synthesis of oleic acid functionalized Fe3O4 magnetic nanoparticles and studying their interaction with tumor cells for potential hyperthermia applications. Coll. Surf. B BIointerfaces 108, 158–168.
Karade, V.C., Sharma, A., Dhavale, R.P., Dhavale, R.P., Shingte, S.R., Patil, P.S., Kim, J. H., Zahn, D.R.T., Chougale, A.D., Salvan, G., Patil, P.B., 2021. APTES monolayer coverage on self-assembled magnetic nanospheres for controlled release of anticancer drug Nintedanib. Sci. Rep. 11, 5674.
Lee, W.S., May Chua, A.S., Yeoh, H.K., Ngoh, G.C., 2014. A review of the production and applications of waste-derived volatile fatty acids. Chem. Eng. J. 235, 83–99.
Li, X., Xue, K., Yang, J., Cai, P., Zhang, H., Chen, H., Cheng, C., Li, Z., 2023. Experimental study on liquid-gas phase separation driven by pressure gradient in transport membrane condenser. Energy 282, 128749.
López-Garzón, C.S., Straathof, A.J.J., 2014. Recovery of carboxylic acids produced by fermentation. Biotechnol. Adv. 32, 873–904.
Luque, L., Westerhof, R., Van Rossum, G., Oudenhoven, S., Kersten, S., Berruti, F., Rehmann, L., 2014. Pyrolysis based bio-refinery for the production of bioethanol from demineralized ligno-cellulosic biomass. Bioresour. Technol. 161, 20–28.
Masur, S., Zingsem, B., Marzi, T., Meckenstock, R., Farle, M., 2016. Characterization of the oleic acid/iron oxide nanoparticle interface by magnetic resonance. J. Magn. Magn. Mater. 415, 8–12.
Mazumder, A., Chowdhury, Z., Sen, D., Bhattacharjee, C., 2020. Electric field assisted membrane separation for oily wastewater with a novel and cost-effective electrocoagulation and electroflotation enhanced membrane module (ECEFMM). Chem. Eng. Process. 151, 107918.
Nistor, C.L., Ianchis, R., Ghiurea, M., Nicolae, C.A., Spataru, C.I., Culita, D.C., Cusu, J.P., Fruth, V., Oaneca, F., Donescu, D., 2016. Aqueous dispersions of silica stabilized with oleic acid obtained by green chemistry. Nanomaterials 6, 9.
Nor, N.M., Arivalakan, S., Zakaria, N.D., Nilamani, N., Lockman, Z., Razak, K.A., 2022. Self-assembled iron oxide nanoparticle-modified APTES-ITO electrode for simultaneous stripping analysis of Cd(II) and Pb(II) Ions. ACS Omega 7, 3823–3833.
Olariu, C.I., Yiu, H.H.P., Bouffier, L., Nedjadi, T., Costello, E., Williams, S.R., Halloran, C. M., Rosseinsky, M.J., 2011. Multifunctional Fe3O4 nanoparticles for targeted bi-modal imaging of pancreatic cancer. J. Mater. Chem. 21, 12650–12659.
Patel, A., Mahboubi, A., Horvath, I.S., Taherzadeh, M.J., Rova, U., Christakopoulos, P., Matsakas, L., 2021. Volatile Fatty Acids (VFAs) generated by anaerobic digestion serve as feedstock for freshwater and marine oleaginous microorganisms to produce biodiesel and added-value compounds. Front. Microbiol. 12, 614612.
Pinelli, F., Saadati, M., Zare, E.N., Makvandi, P., Masi, M., Sacchetti, A., Rossi, F., 2023. A perspective on the applications of functionalized nanogels: promises and challenges. Int. Mater. Rev. 68, 1–25.
Qiao, L., Chen, H., Yu, J., 2023. Recovery of lithium from salt-lake brine by liquid–liquid extraction using TBP-FeCl3 based mixture solvent. Can. J. Chem. Eng. 101, 2139–2147.
Ramos-Suarez, M., Zhang, Y., Outram, V., 2021. Current perspectives on acidogenic fermentation to produce volatile fatty acids from waste. Rev. Environ. Sci. Biotechnol. 20, 439–478.
Reyes, L., Nijitine, C., Vilcocq, L., Fongarland, P., 2020. Green is the new black-A review of technologies for carboxylic acid recovery from black liquor. Green Chem. 20, 8097–8115.
Reyhanitash, E., Kersten, S., Schuur, B., 2017. Recovery of volatile fatty acids from fermented wastewater by adsorption. ACS Sustain. Chem. Eng. 5, 9176–9184.
Reyhanitash, E., Brouwer, T., Kersten, S.R.A., van der Ham, A.G.J., Schuur, B., 2018. Liquid-liquid extraction-based process concepts for recovery of carboxylic acids from aqueous streams evaluated for dilute streams. Chem. Eng. Res. Des. 137, 510–533.
Rozi, S.K.M., Bakhshaei, S., Manan, N.S.A., Mohamad, S., 2016. Superhydrophobic magnetic nanoparticle-free fatty acid regenerated from waste cooking oil for the enrichment of carcinogenic polycyclic aromatic hydrocarbons in sewage sludges and landfill leachates. RSC Adv. 6, 87719–87729.
Sapmaz, T., Mahboubi, A., Taher, M.N., Beler-Baykal, B., Karagunduz, A., Taherzadeh, M.J., Koseoglu-Imer, D.Y., 2022. Waste-derived volatile fatty acid production and ammonium removal from it by ion exchange process with natural zeolite. Bioengineered 13, 14751–14769.
Shehata, A.B., Rizk, M.S., Rend, E.A., 2016. Certification of caffeine reference material purity by ultraviolet/visible spectrophotometry and high-performance liquid chromatography with diode-array detection as two independent analytical methods. J. Food Drug Anal. 24, 703–715.
Shen, X.C., Fang, X.Z., Zhou, Y.H., Liang, H., 2004. Synthesis and characterization of 3-aminopropyltriethoxysilane-modified superparamagnetic magnetite nanoparticles. Chem. Lett. 33, 1468–1469.
van den Bruinhorst, A., Raes, S., Atika Maesara, S., Kroon, M.C., Esteves, A.C.C., Meuldijk, J., 2018. Hydrophobic eutectic mixtures as volatile fatty acid extractants. Sep. Purif. Technol. 216, 147–157.
van Putten, R.J., van der Waal, J.C., de Jong, E., Rasrendra, C.B., Heeres, H.J., de Vries, J.G., 2013. Hydroxymethylfurfural, A versatile platform chemical made from renewable resources. Chem. Rev. 113, 1499–1597.
Wen, F., Zhang, F., Zheng, H., 2012. Microwave dielectric and magnetic properties of superparamagnetic 8-nm Fe3O4 nanoparticles. J. Magn. Magn. Mater. 324, 2471–2475.
Witek-Krowiak, A., Gorazda, K., Szopa, D., Trzaska, K., Moustakas, K., Chojnacka, K., 2022. Phosphorus recovery from wastewater and bio-based waste: an overview. Bioengineered 13, 13474–13506.
Wu, Y., Hu, W., Zhu, Z., Zheng, X., Chen, Y., Chen, Y., 2023. Enhanced volatile fatty acid production from food waste fermentation via enzymatic pretreatment: new insights into the depolymerization and microbial traits. ACS EST Engg. 3, 26–35.
Wu, X., Lei, Z., Li, Q., Zhu, J., Chen, B., 2010. Liquid-liquid extraction of low-concentration aniline from aqueous solutions with salts. Ind. Eng. Chem. Res. 49, 2581–2588.
Xing, T., Yu, S., Tang, J., Liu, H., Zhen, F., Sun, Y., Kong, X., 2023. Liquid-liquid extraction of volatile fatty acids from anaerobic acidification broth using ionic liquids and cosolvent. Energies 16, 785.
Xuan, L., Ju, Z., Skonieczna, M., Zhou, P.K., Huang, R., 2023. Nanoparticles-induced potential toxicity on human health: Applications, toxicity mechanisms, and evaluation models. MedComm. 4, e327.
Yesil, H., Calli, B., Tugtas, A.E., 2021. A hybrid dry-fermentation and membrane contactor system: enhanced volatile fatty acid (VFA) production and recovery from organic solid wastes. Water Res. 192, 116831.
Yin, D.M., Uwineza, C., Sapmaz, T., Mahboubi, A., De Wever, H., Qiao, W., Taherzadeh, M.J., 2022. Volatile Fatty Acids (VFA) production and recovery from chicken manure using a High-Solid Anaerobic Membrane Bioreactor (AnMBR). Membranes 12, 1133.
Yuan, B., Braune, M., Grongroft, A., 2023. Liquid-liquid extraction of caproic and caprylic acid: solvent properties and pH. Chemie Ing. Tech. 95, 1573–1579.

Zacharof, M.P., Lovitt, R.W., 2013. Complex Effluent Streams as a Potential Source of Volatile Fatty Acids. Waste Biomass Valoriz. 4, 557–581.
Zakzeski, J., Bruijnincx, P.C.A., Jongerius, A.L., Weckhuysen, B.M., 2010. The catalytic valorization of lignin for the production of renewable chemicals. Chem. Rev. 110, 3552–3599.
Zhu, X., Xu, Y., Gao, Y., Huang, L., 2012. Pressurized liquid extraction combined with dispersive liquid-liquid micro-extraction as an efficient sample preparation method for determination of volatile components in tobacco. J. Chinese Chem. Soc. 59, 909–916.